AE Applied to Superstructure

Masayasu Ohtsu, Tomoki Shiotani, and Mitsuhiro Shigeishi

Abstract It is evolutionally reported that number of infrastructures, in particular, superstructures constructed and currently in services are aged and deteriorated after long-year service. In the case of concrete structures, fatigue damage due to traffic and corrosion-induced cracks are extensively reported. In the case of steel structures, deterioration mostly occurs due to fatigue cracking, resulting from increasing span length and overloading of traffic vehicles. As presented here, AE measurement has been applied to such superstructures as building, reinforced concrete (RC) bridge, and steel bridge. In addition, innovative applications of AE tomography are discussed. Thus, the deterioration and the damage of superstructures are extensively summarized.

Keywords RC bridge · Girder · Slab · Steel bridge · Deck · Tomography

1 Introduction

Development of highway networks has supported motorization, high economic growth and modernization all over the world. Thus, an enormous number of infrastructures, in particular, buildings and bridges have been constructed. However, many of them are currently known to have been aged and deteriorated after long-year service. In concrete structures, damages due to deteriorated or aged materials including corrosion of reinforcement and poor-workmanship responsible for initial cracking are often reported. Steel structures are deteriorated mostly by fatigue, resulting from increasing span length and overloading of traffic vehicles.

M. Ohtsu (✉) · T. Shiotani
Graduate School of Engineering, Kyoto University, Kyoto 615-8540, Japan
e-mail: ohtsu.masayasu.4v@kyoto-u.ac.jp

T. Shiotani
e-mail: shiotani@df7.so-net.ne.jp

M. Shigeishi
Faculty of Advanced Science and Technology, Kumamoto University, Kumamoto 860-8555, Japan
e-mail: shigeishi@civil.kumamoto-u.ac.jp

C. U. Grosse et al. (eds.), *Acoustic Emission Testing*, Springer Tracts in Civil Engineering, https://doi.org/10.1007/978-3-030-67936-1_12

According to the standard specifications for concrete structures (JSCE 2001), the maintenance and management are explained in the following.

Step 1: Inspection,
Step 2: Evaluation of inspected results,
Step 3: Prediction by deterioration model, and
Step 4: Counter-measures for maintenance and management.

Thus, inspection procedures for the maintenance and management of structures are of fundamental importance prior to making a prediction model for deterioration and deciding counter-measures for repair and retrofit. The procedures could become diagnostic standards for evaluating the structural integrity.

There exist various methods for inspecting superstructures in service. So far, a visual inspection is most extensively employed. Since defects, deterioration, and damage normally grow inside structure, a safety assessment cannot be based solely on the visual observation of cracks and signs of damages in structural elements. The technique should enable to provide definitive and quantitative evaluation in a short time. In this respect, a variety of nondestructive evaluation (NDE) methods are being under investigation and in progress for practical use.

For diagnosis in superstructures of concrete and steel, applications of AE techniques are in progress. AE method is expected to become a very useful technique for evaluating the soundness and for detecting damages of the superstructure. This is because the measurement can be carried out without stopping traffic in a bridge or without evacuation of residents in a building. Here, successful results on the applications to buildings and bridges are stated. In association with an innovative applications of AE tomography, a promise for diagnosis and monitoring in the superstructures is discussed.

2 Building

For AE monitoring of existing concrete structures, it is essential to confirm that any AE signals responsible for the deterioration are not observed under service conditions. In the case that AE signals not of noises but due to deterioration process are detected, the monitoring and the analyses shall be conducted. The monitoring is performed continuously or routinely, and sometimes temporarily after the disasters. In this case, the selection and classification of AE signals which is closely associated with the deterioration are necessary.

In a historical masonry building, the efficiency of AE technique to monitor cracking is reported (Carpinteri and Lacidogna 2006). Comparing crack traces and AE activity, it is shown that AE measurement can be used to dynamically measure structures in service.

In an old reinforced concrete building, AE measurement was carried out in advance of rebuilding the house. A plan view of the two-story building is given in Fig. 1. Since the structure was old and not in service, the audible noises were readily observed

due to the traffic load. At five locations circled in the figure, continuous monitoring was conducted for a week. To analyze AE data, two waveform parameters of the RA value and the averaged frequency stated in Chapter 4 Parameter Analysis were applied.

Following ISO standard (ISO16838 2019), cracks are readily classified into tensile and shear cracks from two parameters as shown in Fig. 2. In the figure, R3, R6, and R15 represent the data detected with AE sensors of the resonance frequencies 30 kHz, 60 kHz, and 150 kHz, respectively. This implies that results are not dependent on characteristics of the sensors.

Results of the classification are given in Fig. 3. Locations of the observation are labeled by the numbers from north to south and by the capital letter denoted from the left to the right as given in Fig. 1, and then the floor number is appended. As an example, 1A1 denotes the north-the left corner of the building at the fist floor. In the figure, AE waveforms are classified into a tensile type and a shear type based on the criterion in Fig. 2. High AE activities are observed at four locations 1B1, 1D1, 4E1 and 4D2. To investigate the conditions of concrete, core samples were take out after AE measurement from every location.

Then internal defects such as a cavity or a honeycomb were found at several locations, which are indicated by the letter "D". It is found that locations 1B1, 4E1 and 4D2 are indicated as defected, where AE waves of shear type are mostly observed. This implies that AE events were generated due to fretting of concrete at these defects. At one location 1D1, in contrast, tensile cracks are dominantly observed. Thus, it was concluded that tensile cracks were newly nucleated and extending at this location.

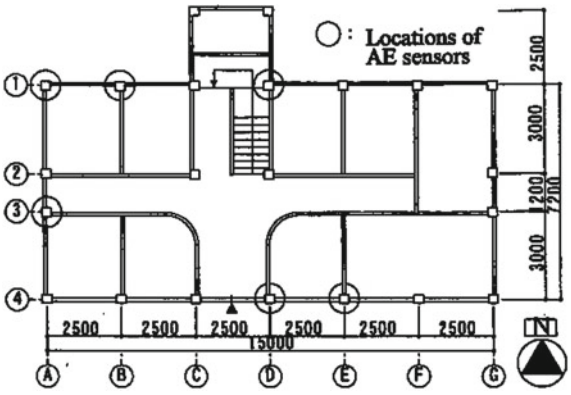

Fig. 1 Plan view of a reinforced concrete building

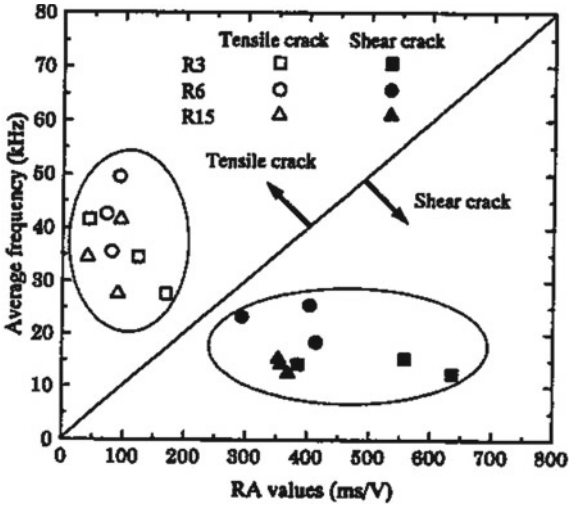

Fig. 2 Classification of crack types

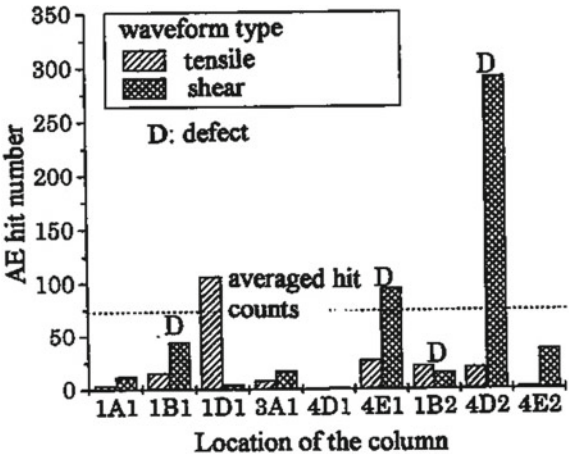

Fig. 3 AE events and locations

3 Concrete Bridge

3.1 RC Girder

In order to establish the procedure applicable to actual bridges of about 10–100 m length, AE measurement was conducted in a bridge, of which girders were replaced (Shigeishi and Ohtsu 2004). A reinforced concrete (RC) girder bridge with a cross-section of T-shape is shown in Fig. 4 that was in service for about 45 years. All girders were dismounted for replacement, and one girder in the figure was tested.

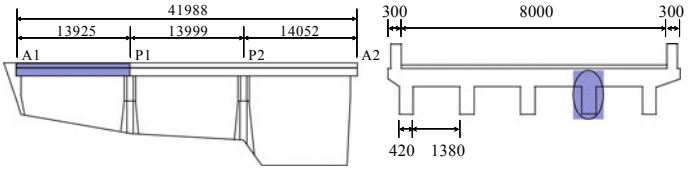

Fig. 4 A view of a road bridge in service

Fig. 5 Test set-up for the cyclic bending test in a dismantled girder

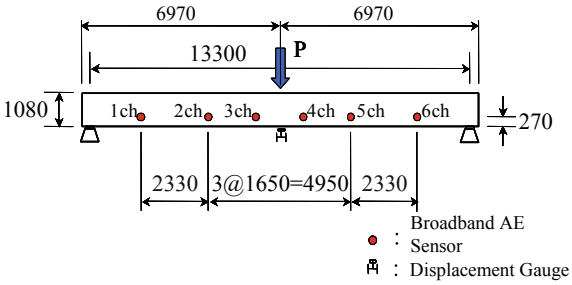

AE generating behavior under a repetitive bending-load was measured, applying a large loading device.

A sensor array and a loading condition are illustrated in Fig. 5. The purpose of this test was to investigate the Kaiser effect in a real-scale member.

In the loading test, the bending load is applied by using the steel frame shown in Fig. 6. A hydraulic jack is placed at the top center between two supports of the girder. The loading force is measured by a pressure gauge inserted between the jack and a loading bar along with a deflection gauge installed right below the loading section. Six broadband-type AE sensors (UT1000, PAC) are attached on one side at the web of the girder as shown in Fig. 5. Output signals from AE sensors are amplified by 40 dB gain and the detection threshold is set to 38 dB referring to the sensor output.

As seen in Fig. 7, under a cyclic-incremental loading, the gradual increase of total number of AE hits was observed. From the both graphs, the Kaiser effect can be observed until the loading cycle of 150 kN, because a few AE hits are only observed and no increase in unloading cycles. Once the maximum repetitive load exceeded 200 kN, AE activity was observed even below the maximum previous load and tended to increase in unloading stages.

Thus, it is demonstrated that the Kaiser effect is observed in a full-scale girder. For the comparison with AE results, residual deformations at the center of the girder are shown in Fig. 8.

The deformations increase continuously with the increase in loading stages. Thus, no clear transition is observed at the load level of 200 kN, where the deformation exceeds 1.0 mm. Concerning the serviceability of the superstructure, deformations less than 2 mm are not critical, but AE observation suggests the beginning of deterioration over 200 kN cycles as the breakdown of the Kaiser effect.

Fig. 6 Loading device for a bending test of the girder

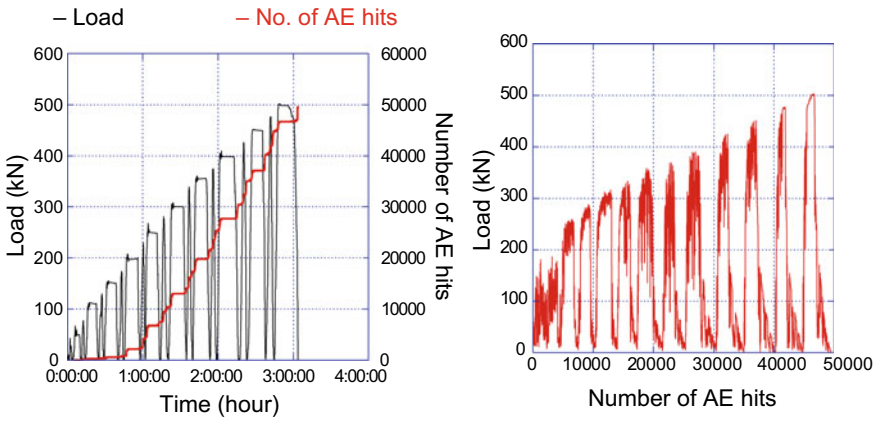

Fig. 7 AE generation behavior and loading cycles of the dismantled girder in a cyclic bending test

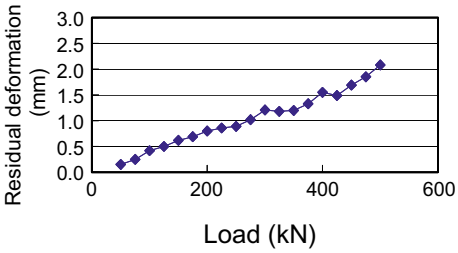

Fig. 8 Residual deformations at the center of the girder

In relation with the Kaiser effect, ISO standard (ISO16837 2019) presents a guideline to qualify the damage of reinforced concrete (RC) structures. Thus, a feasibility of the practice is studied. The Kaiser effect means the phenomenon that a material under load emits AE waves only after a primary load level is exceeded. During reloading, the material behaves elastically before the previous maximum load is reached. The effect suggests that little or no AE events are recorded before the previous maximum stress level is achieved. However, the effect comes to be vanished after the material once suffers from serious damages. In the definition of the Felicity effect, nucleation of the plastic zone in the material is suggested to be a cause for disappearance of the Kaiser effect. Based on these findings, two indices are newly proposed as the load ratio and the calm ratio, as stated in chap. "Parameter Analysis". A schematic illustration is given in Fig. 9.

The load ratio and the calm ratio were estimated in the test of the dismantled girder. Results are shown in Fig. 10. It is clearly observed that with the increase in loading cycles, plotted points move from the sound zone to the serious damaged zone. The zones classified are not yet clearly described with threshold values, because these values are to be specified from experiments data of structural members. In the case of the present test, the loading cycle up to 200 kN is to be one threshold value. Thus, the usefulness of ISO rstandard is confirmed. Data acquisition on RC girders

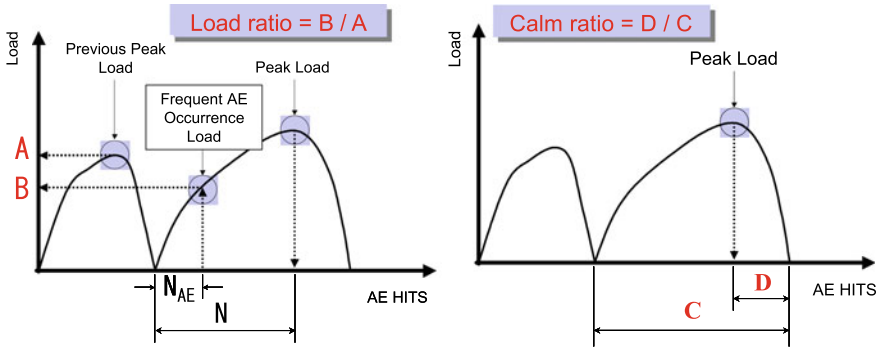

Fig. 9 Definitions of load ratio and calm ratio in a cyclic loading

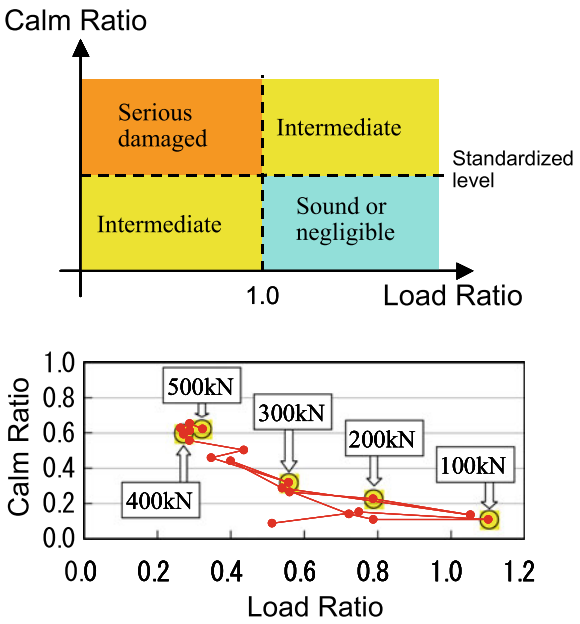

Fig. 10 Diagram of the load ratio and the calm ratio during the test

is promising to establish the criterion for the damage qualification of many kinds of RC structures.

3.2 RC Slab

In the previous section, a full-scale girder was tested to qualify the damage. However, the main members of a superstructure seldom receive the extreme damage, except in accidents or after earthquakes. Results of the Inspection often report defects of local areas. At such parts subject to intensive repetitive stresses as floor slabs and bearings, serious damages are detected due to traffic loads in service. So, results of AE monitoring at a slab of a RC bridge are given.

The measurement is conducted in the bridge on a general highway in an urban area shown in Fig. 11 (Shigeishi et al. 2003). In the measurement, AE parameters are recorded at the sensor output ratio of 42 dB as the threshold by using an AE signal waveform analyzer. 6-channel analog signal processing system is employed with six broadband AE sensors and 40 dB preamplifiers.

Between piers P1 and P2 of the four-span bridge, AE sensors are arranged at the transverse beam as shown in Fig. 11. The sensors are set at interval of 1350 mm along the bridge axis at the center between the floor slab supports. The line selected for sensor arrangement corresponds to the line where the right-side wheels of vehicles run. In a test, heavy vehicles crossed the bridge under traffic control as shown in Fig. 12, and AE signals are recorded.

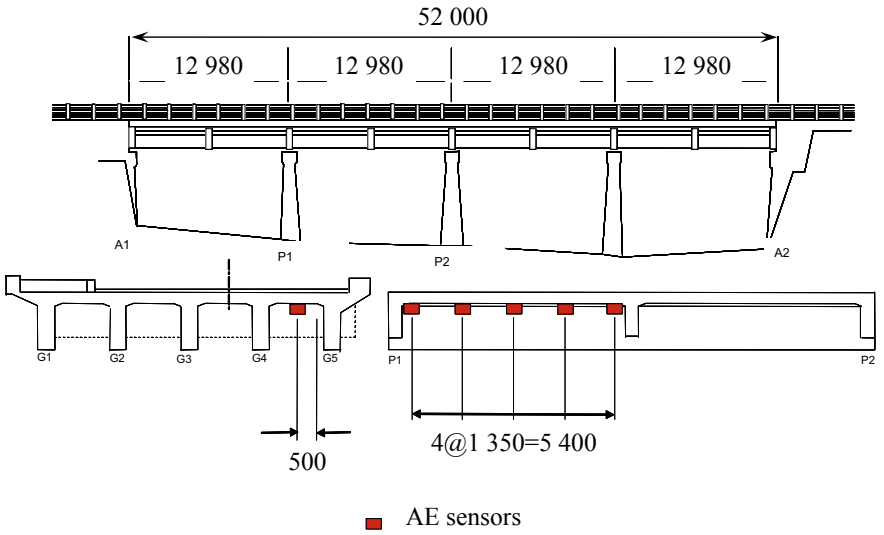

Fig. 11 AE monitoring on a slab of a road bridge

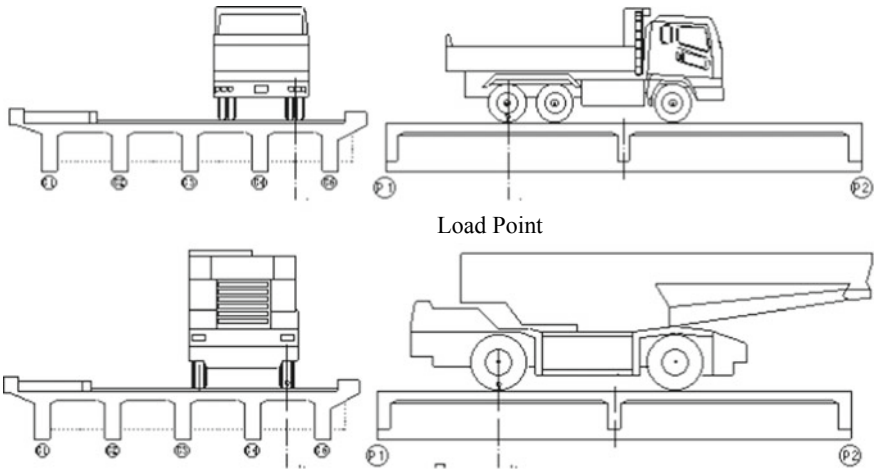

Fig. 12 AE measurement under heavy-vehicle loading

When the vehicles moved at the normal speed of about 40 km/h, total AE energy detected by each channel is shown in Fig. 13. In the left figure, results of one-dimensional location are also given as cumulative AE events. It is observed that AE energy detected at channel 1 is remarkably large, probably because the sensor of channel 1 is close to the joint of pier P1 where wheels of vehicles could convey impact loads on the slab crossing over the joint. AE energy decreases as reaching

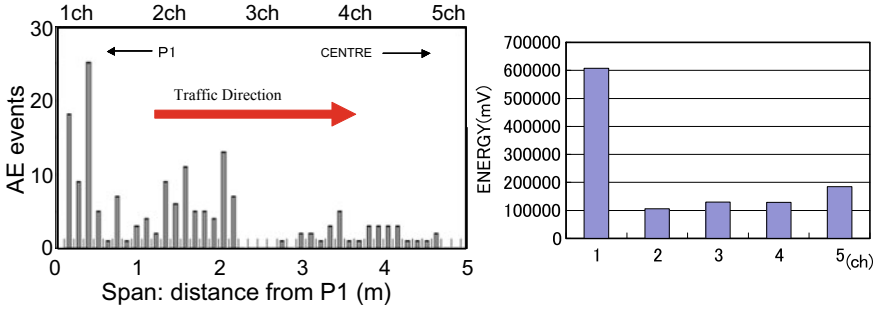

Fig. 13 Cumulative AE events and AE energy under traffic load (40 km/h)

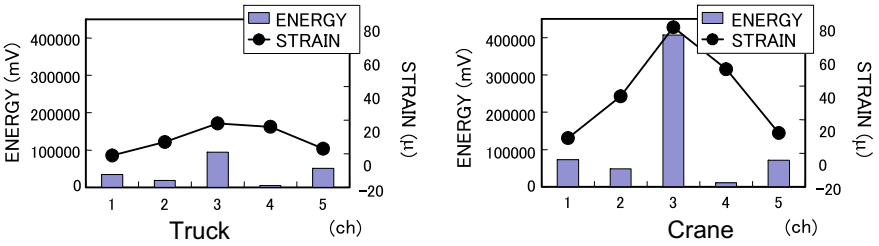

Fig. 14 AE energies and strains at rebar observed under slow heavy-load traffic (V = 20 km/h)

to channel 5. This is because deformations at the central area are elastic enough as indicating the soundness state.

In Fig. 14, total AE energy at each channel is compared with strain measured at reinforcing-steel rod under the slow-speed running (V = 20 km/h) of a dump truck and a rafter crane. Both AE energy and the strain are highest at the position of channel 3. These are results obtained under slow-running traffic. Thus, AE activity and the strain at channel 1 are smaller than those of channel 3. Compared with AE activity in Fig. 13 observed while the bridge is in service, distribution of AE energy is fairly different. This is because vehicles moved at low speeds and did not produce impact loads at the joints.

In Fig. 15, total AE energy and strain at reinforcing rod by each channel are shown. These were observed under very slow loading (almost static condition: V = 5 km/h). Concerning the strains at reinforcing rods, the values become larger at channel 1 and channel 5 than those of other locations. The energy also became greater at channel 1 and channel 5. Considering the observed distributions of AE energy, it is found that the impact load generates AE events near the joint, slow-moving load generates a low-frequency vibration associated with AE activity at channel 3, and AE activity due to quasi-static loading is similar to a bending-moment distribution under uniform load.

From in-situ inspection of existing concrete bridges, it is clarified that the running speed of vehicles should be taken into consideration in the measurement. Otherwise,

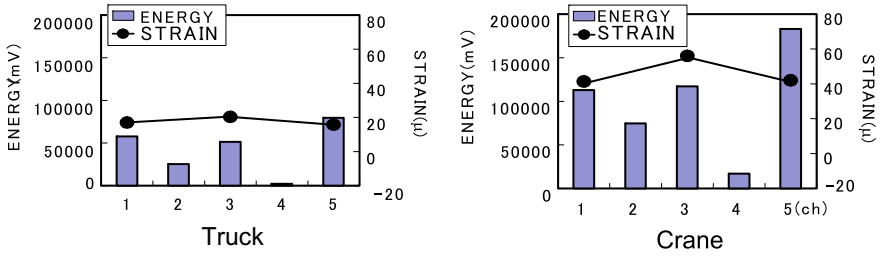

Fig. 15 AE energies and strains under quasi-static heavy loading (V = 5 km/h)

the damaged zone might not be correctly identified, because the impact loading could generate high AE activity at the joints. In other cases, vibration modes due to moving loads may affect AE activities at local areas.

4 Steel Bridge

Steel bridges are generally employed for longer spans than concrete bridges. With the recent trend for large bridges, the superstructures are not only made of steel frame, but also reduce their weights by adopting steel slabs. Currently, complicated floor framing composed of relatively small steel members has so many jointed or welded sections where initial defects are afraid to affect the durability, in particular, the fatigue cracking. Due to the increase in unpredictable of traffics and overloaded vehicles, severe damage in small steel members are highly concerned.

In a large bridge of steel box-girders shown in Fig. 16, cracks are visually found. Consequently, the activities of cracks are estimated by the AE method (Shigeishi 2004). The slab is covered with a waterproof resin sheet and asphalt was directly layered above the sheet. During the measurement, the bridge was in service, carrying traffic.

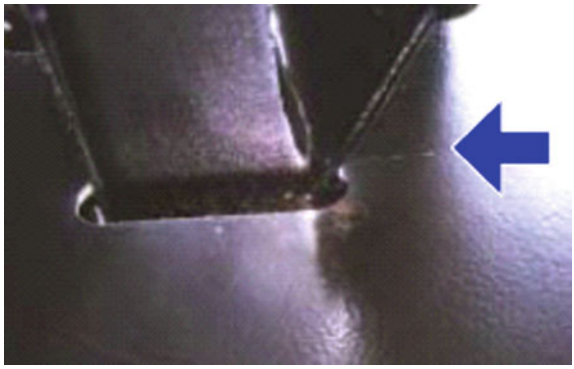

Fig. 16 Photo of a fatigue crack propagating from a weld line with a lateral beam through U-shaped rib stiffener

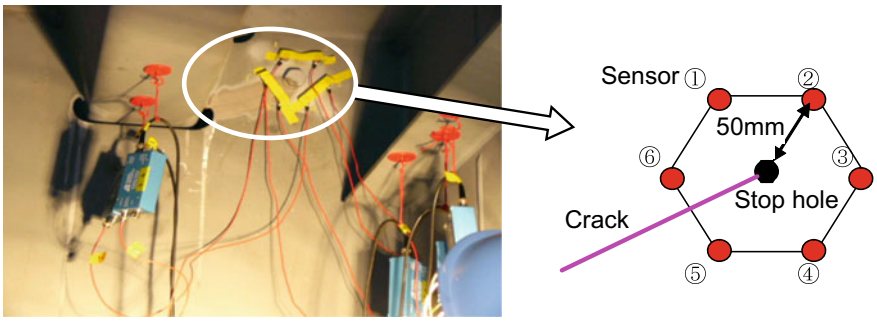

Fig. 17 AE measurement on lateral beam connecting with U-shaped rib plate

In Fig. 17, sensor array is shown for AE measurement on a welded section of a steel-slab connecting with a lateral beam. By applying a ultrasonic test (UT), a crack is suspected at a location where the U-shaped rib plate is welded with the lateral beam. AE sensors are installed to locate sources around the stop-hole to arrest crack extension.

Six AE sensors of 150 kHz resonance-type (R15, PAC) are attached on the side of the lateral beam. As a result, AE sources are located around the hole as shown Fig. 18. High AE activity may indicate that a latent crack is propagating due to traffic load.

Then AE sources are also located by installing guard sensors as shown in Fig. 19. The guard sensors are employed to discriminate from sources originating from outside the area of interest. Because waves from outside the area can be detected at least one of the guard sensors (1, 2 or 3 shown in Fig. 19) before arriving at the sensor (4, 5 or 6) placed on the area of interest, this technique is applicable to reject

Fig. 18 AE sources located during the measurement

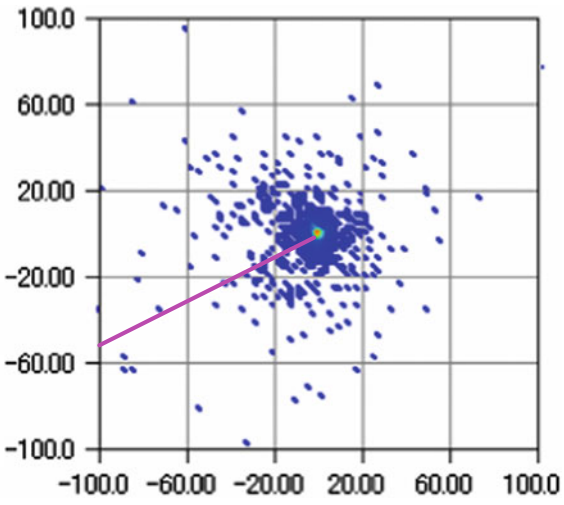

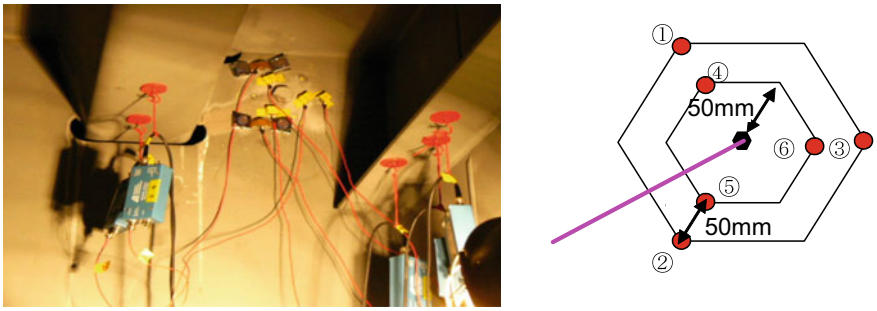

Fig. 19 AE measurement with guard sensors

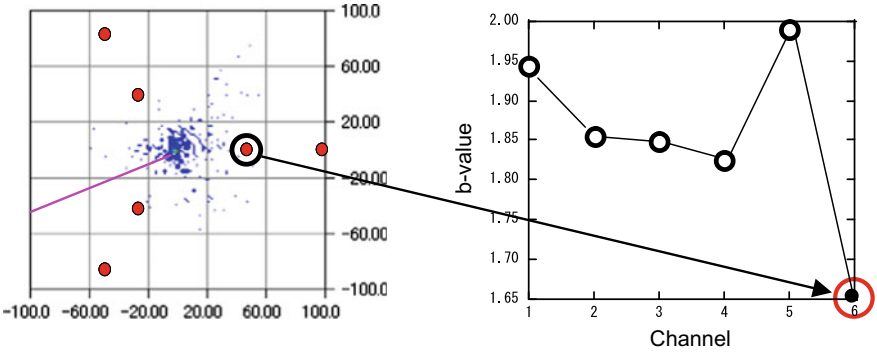

Fig. 20 AE sources located by guard sensors and b-values at 6 channels

the noise from the outside. From the locations in Fig. 20, we can identify a probable crack-tip around AE cluster.

In Fig. 20, the b-values observed at 6 sensors are given. As can be seen from the graph, the b-value is remarkably small at AE sensor at channel 6 where the edge of AE cluster is identified in comparison with the b-values at the other AE sensors. This seems to suggest an orientation of probable crack propagation, because generation of large-scale AE events is identified from the b-value observed at channel 6.

5 Steel–Concrete Composite Slab

A steel–concrete composite slab is newly available in construction, of which concrete is placed in a steel mold that consists of steel side plates, top reinforcing bars and transverse ribs, and stud-planted bottom steel plates. Configuration of one type slab is shown Fig. 21. Compared with a reinforced concrete slab, this slab is expected to bear a large load- capacity and to have good endurance. Although these characteristics are

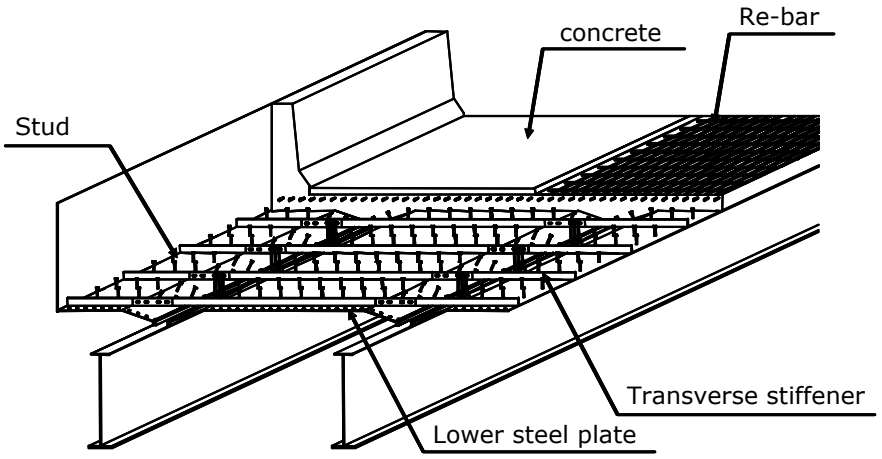

Fig. 21 Robinson-type of steel–concrete composite slab

favorable for bridge construction, visual inspection is very difficult in particular, for concrete and its interface with steel plate. As a result, effective inspection techniques for steel–concrete composite slabs are in demand and under development.

Applying the AE method, cyclic tests of repetitive loading and fatigue loading are conducted (Itoh et al. 2002). The case where delamination between concrete and steel plate occurs is investigated, which is regarded as one of the serious deterioration mechanisms in composite floor slabs. The fracture of studs and the fatigue damage of concrete are also examined from AE results.

A Robinson-type steel–concrete composite floor slab is of dimensions of 1540 mm × 159 mm × 1500 mm, which is shown in Fig. 22. To withstand deflections due to concrete casting, transverse ribs are arranged at the center and on both sides.

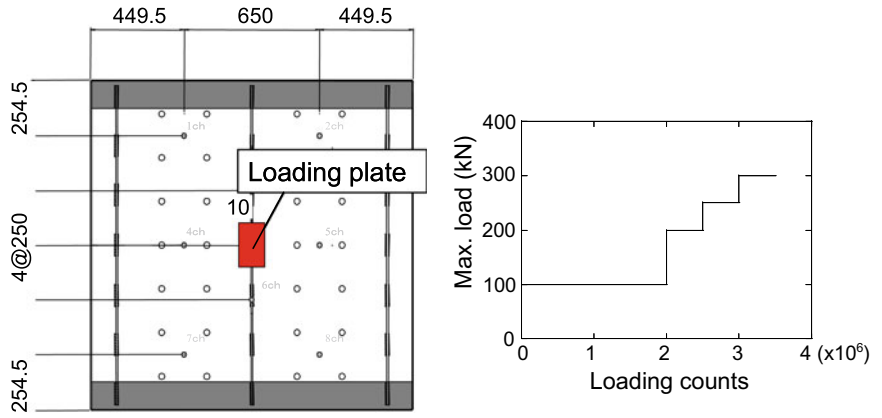

Fig. 22 Steel–concrete slab specimen and fatigue loading steps

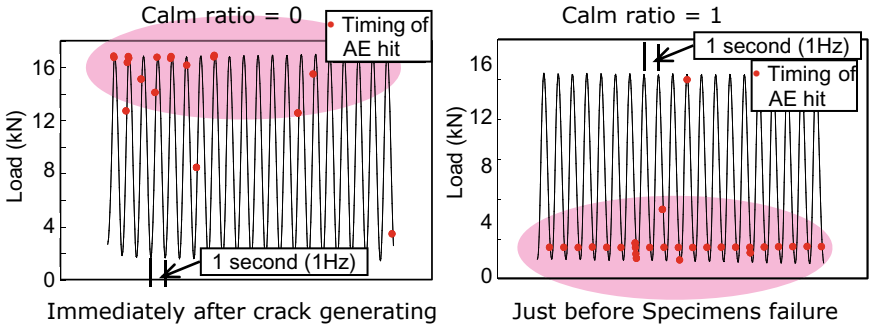

Fig. 23 AE generating behaviors and the calm ration during cyclic loading

The loading position is set at the top center of the specimen. A plate of dimensions 200 mm × 125 mm is installed as a loading plate. Load of 100 kN is first applied 2 million times at a frequency of 3 Hz, then 250 kN is applied 0.5 million times at 2 Hz, and finally 300 kN is applied 0.5 million times at 1 Hz.

AE sensors are arranged on the bottom steel slab. Following every 10,000 times loading, AE events generated during 300 times of loading are recorded. In Fig. 23, some of results after surface cracks are observed in concrete and at a final stage are shown. Before 2 million times of loading, AE events are actively observed when the deflections under the load position starts increasing acceleratedly. After 2 million times of loading, AE events are observed at unloading cycles. As seen in the left graph, the calm ratios are equal to zero until cracks were nucleated. Approaching the final stage, the calm ratios become 1.0 as found in the right graph. Therefore, it suggests that the calm ratio is applicable to estimate the soundness of the steel–concrete composite slab in AE measurement, even though visual inspection is not available.

6 Application of Tomography to RC Deck Panel

For a real-time monitoring and quantitative evaluation of the level of damage in the superstructures, AE and the tomography are known to be promising (Behnia 2014).

In-situ AE measurements of RC decks are conducted for a week (Shiotani et al. 2018). Internal damage of an RC deck panel is evaluated first by AE source locations. Then, distribution of elastic-wave velocities are evaluated by means of AE tomography.

6.1 Procedure of AE Tomography

In the analytical procedure of the elastic-wave tomography, an impact is generated at the sensor, and elastic-waves are detected at other sensors. In the case of AE tomography, detections of elastic waves are identical, while the driving impact is replaced by AE sources or artificial excitations as hammering. After each arrival time is obtained, the propagation velocity is determined from the propagation path, crossing element meshes. In the algorithm, the inverse of the velocity is referred to as the "slowness". A theoretical propagation time is obtained, as a total of the propagation time calculated by the slowness and the distance in each element. The difference between observed propagation time and theoretical propagation is calculated. Then, the slowness in each element is revised in order to reduce the difference. Eventually, the velocity of each element is determined, following the iteration procedure. Through the procedure, a distribution of velocities are determined in the target area. It is noted that in AE tomography, locations of AE sources and the velocity distribution are simultaneously determined after the iteration procedure.

6.2 AE Activity and Tomography in RC Deck

An RC bridge deck is selected as a target, in which rebar corrosions due to salt attach and fatigue cracks due to heavy traffic have been identified as a major deterioration. AE measurement is carried out with AE sensors, set on the bottom side of the decks. Resonant frequency of the AE sensor is 30 kHz, arranged on the RC deck as shown in Fig. 24.

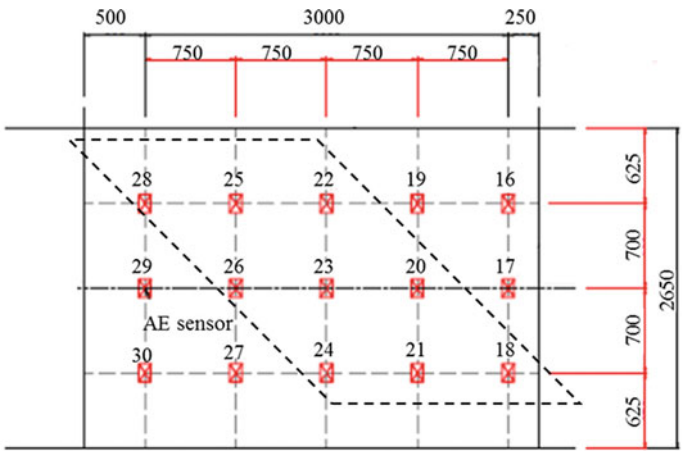

Fig. 24 Sensor arrangements for AE measurement on in-situ RC bridge decks

Thickness of the RC bridge decks is 235 mm. Serious damage could be expected for the deck, since large cracks with water leakage are observed. A threshold value of location uncertainty (LUCY) is set on 300 mm, about half space of two adjacent sensors, where LUCY means the source location accuracy and is estimated as the root-mean-square of the difference between calculated and observed distances between the source and the sensor (Hamstad 2007).

Dotted lines of parallelogram in Fig. 24 shows the cut-off panel to be investigated, where three-dimensional (3D) analysis of the tomography is carried out to estimate velocity distributions inside of the panel. AE sensor array for the tomography analysis is illustrated in Fig. 25.

12 sensors of 60 kHz resonance are additionally set on the bottom of the panel. Random excitations with a hammer of 11 mm curvature edge are made for generations of the waves on the top surface of the panel. Appropriate input sources are carefully selected with such conditions, as the number of hits for one AE event is more than five by one hammering and LUCY is shorter than 300 mm. Results of AE tomography are shown in Fig. 26 with AE sources located and classified with peak amplitudes of the first arrival of AE events.

In general, the area over the velocity of 4000 m/s suggests sound condition, while that of lower than 3000 m/s possibly implies serious damage. As can be seen, the areas of low velocity show less AE activity. In contrast, the areas of high velocity denote intensive AE activity. By means of core-drilled sampling, these results are

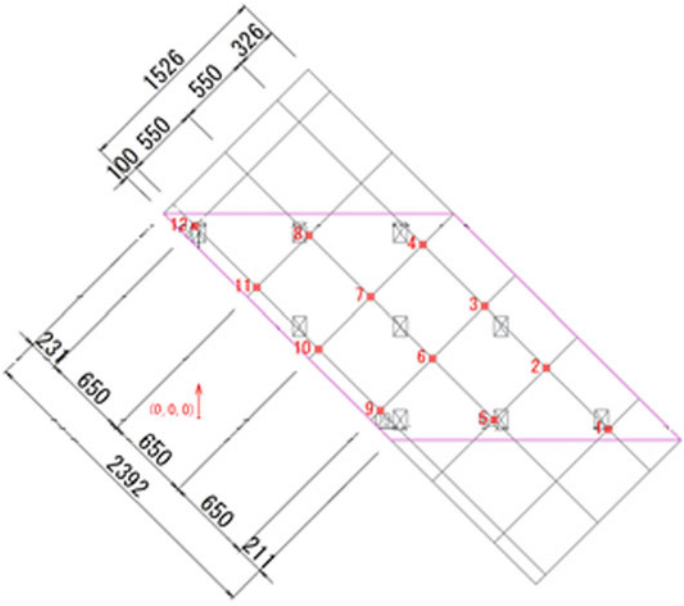

Fig. 25 Sensor arrangement in random hammering for AE tomography (Unit: mm)

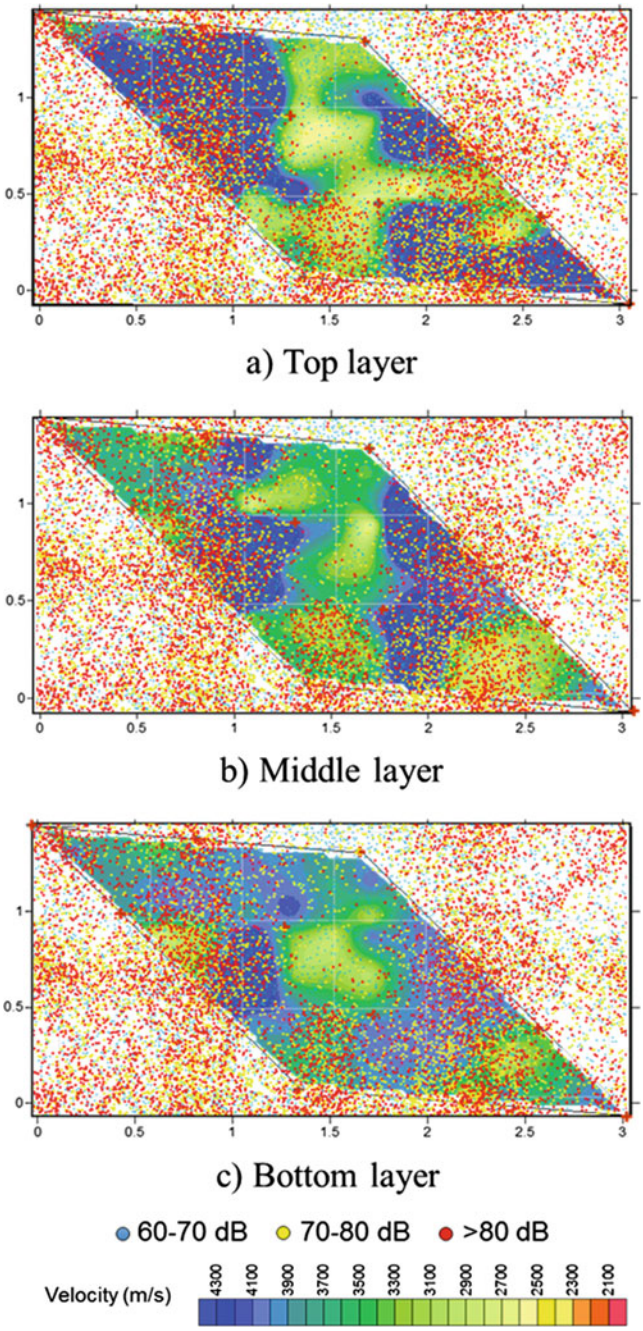

Fig. 26 Velocity distributions from the top to the bottom of RC deck with AE source locations classified with peak amplitudes of the first arrival of AE events

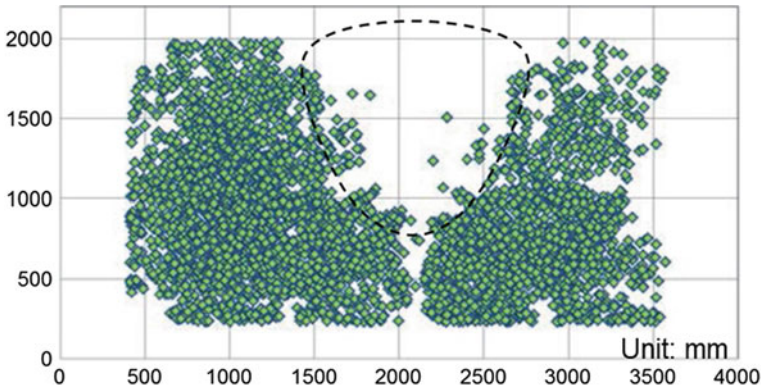

Fig. 27 Result of AE source location analysis

investigated. It is confirmed that cores in the area of low velocity with less AE activity contain serious damage. The fact may result from an attenuation property of elastic waves in the damaged area.

6.3 AE Activity Due to Rain

In order to develop a new damage assessment in superstructures in service, AE activity induced by rain droplets in a short period of minutes are investigated (Takamine et al. 2017; Watabe et al. 2018). As an example, AE events are recorded in the same deck during a heavy rain, and the source locations analysis is performed. One result is shown in Fig. 27. Here, the source locations considered as low reliability are filtered out. As a result, AE sources are analyzed only for 700 s. In the figure, a low-density area of AE clusters surrounded by broken curve is observed, although randomly distribution due to precipitation is expected.

Thus, the presence of the low AE activity area is studied, applying AE tomography to rain-induced AE sources. Results are given in Fig. 28, along with core samples taken out of the deck. As shown in the figure, horizontal cracks are observed in the cores at the area of low AE activity, which clearly corresponds to the low velocity zone. It is noted that this is not exactly true for the core samples C11 and C13 which are both located at the border between the low velocity zone and the medium velocity. These minor inaccuracies may result from the fact that the fineness of the mesh determining elements of the tomography analysis is not precisely associated with a rigorous evaluation or the effect of secondary damage produced during cut-off work.

Comparing the velocity distributions in Fig. 26 with those in Fig. 28, a reasonable agreement is observed. This implies that AE events produced by the precipitation

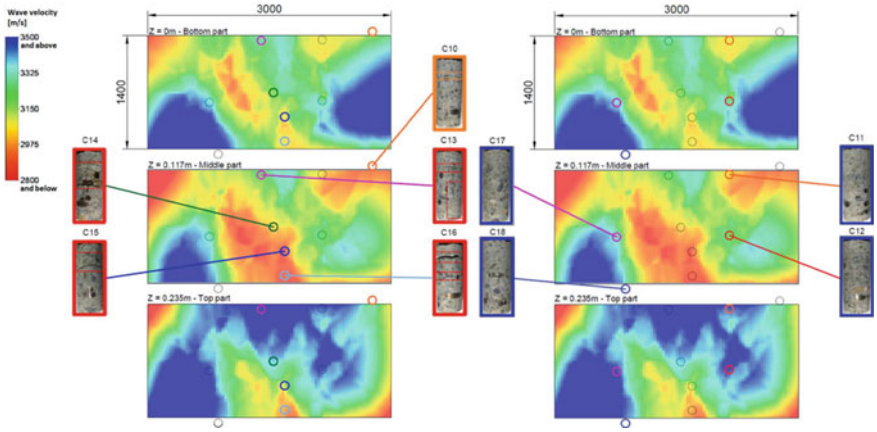

Fig. 28 Comparison between the tomograms and the core samples

in a short-term provides useful tomogram results, being compatible to those of AE events due to the damage in a long-term.

7 Concluding Remarks

AE measurement has been applied to the superstructures to evaluate the deterioration and the damage. In the case, in situ measurement under service or traffic loads is essential. With the all findings, it is suggested that the prompt decision could be readily made on the issues, whether slabs and decks shall be replaced, repaired or left.

In addition, AE activity induced by rain droplets in a short period are identified by AE source location. Through the evaluations, it is found that the distribution of AE sources induced by precipitation could reflect internal damage of RC slabs i.e., dense areas of source locations imply the intact or minor damage, while sparse areas of source locations suggest serious damage of RC decks.

In these applications, the care for environmental noises is essential. This is because the measuring conditions at the site are varied one by one. It is quite important to conduct preliminary tests prior to actual tests on equipment setting and measuring conditions. Based on these well-cared preparations, valuable AE data are to be successfully obtained.

References

Behnia A, Chai HK, Yorikawa M, Terazawa M, Shiotani T (2014) Integrated non-destructive assessment of concrete structures under flexure by acoustic emission and travel time tomography. Construct Build Mater 67(PART B):202–215

Carpinteri A, Lacidogna G (2006) Damage monitoring of an historical masonry building by the acoustic emission technique. Mater Struct 39:161–167

Hamstad MA (2007) Acoustic emission source location in a thick steel plate using lamb modes. J Acoust Emiss 25:194–214

ISO16837 (2019) Non-destructive testing—acoustic emission inspection—test method for damage qualification of reinforced concrete beams

ISO16838 (2019) Non-destructive testing—acoustic emission inspection—test method for classification of active cracks in concrete structures

Itoh T, Shigeishi M, Ohtsu M (2002) Acoustic emission in fatigue process of steel plate-concrete composite slab. Prog Acoust Emiss 11:132–137

JSCE (2001) Standard specifications for concrete structures: maintenance. Japan Society of Civil Engineers, Tokyo

Shigeishi M, Makizumi T, Jo H, Ueda J (2003) AE monitoring of a reinforced concrete road bridge. In: Structural faults and repair 11 (CD-ROM): NDTB-SHIG

Shigeishi M, Ohtsu M (2004) Applicability of damage estimation based on acoustic emission activity under loading to practical reinforced concrete bridge. Bridge Mainten Safety Manage Cost (CD-ROM) 797–798

Shigeishi M (2004) A report of the development of acoustic emission application for inspection of bridge superstructure. A material of the technical committee on acoustic emission. Jpn Soc Non-Destruct Test 121:15–22

Shiotani T, Hashimoto K, Asaue H, Watabe K, Fukuda M (2018) Lateral damage identification in RC slabs by several tomographic approaches with rainy induced elastic waves. J Mech Eng 64(11):657–664

Takamine H, Watabe K, Miyata H, Asaue H, Nishida T, Shiotani T (2018) Efficient damage inspection of deteriorated RC bridge deck with rain-induced elastic wave. Constr Build Mater 162:908–913

Watabe K, Takamine H, Nishida T, Shiotani T (2017) Novel non-destructive technique of internal deterioration in concrete deck with elastic wave approaches. In: Asset intelligence through integration and contemporary vibration engineering technologies, p 665